Journal of Materials Chemistry A

ROYAL SOCIETY OF CHEMISTRY

PAPER

View Article Online
View Journal | View Issue

Cite this: *J. Mater. Chem. A*, 2024, **12**, 4846

Large transverse magneto-thermoelectric effect in narrow-band-gap polycrystalline $Ag_{2-\delta}Te$†

Mingyu Chen, ‡[ab] Tao Feng,‡[c] Nan Yin,[d] Quan Shi, [d] Peng Jiang *[ad] and Xinhe Bao *[ad]

Received 30th November 2023
Accepted 16th January 2024

DOI: 10.1039/d3ta07394g

rsc.li/materials-a

To achieve practical applications of transverse thermoelectricity, it is essential to discover novel high-performance polycrystalline transverse magneto-thermoelectric materials. Herein, we find that polycrystalline $Ag_{2-\delta}Te$ exhibits a peak Nernst thermopower of 625 μV K^{-1} at 75 K under a magnetic field of 14 T. Such a high value might originate from the enhanced bipolar effect and the crossed linear band near the low-temperature N–P transition. Our studies suggest the promising potential of Ag_2Te-based materials for energy conversion utilizing the Nernst effect and open up a new avenue for the development of novel magneto-thermoelectric materials.

Introduction

Thermoelectricity plays a crucial role in solid-state waste-heat harvesting and cooling, as it enables the direct conversion of electricity into heat and *vice versa* without mechanical components and greenhouse gas emissions.[1–3] In recent years, significant advancements have been made in traditional thermoelectric materials by band engineering, such as band convergence,[4–6] band flattening,[7] or phonon engineering, including nano-inclusions[8,9] and grain boundaries.[10–12] Additionally, the application of an external magnetic field offers an additional strategy for optimizing thermoelectric performance.[13] In general, magneto-thermoelectric (MTE) effects encompass both longitudinal and transverse components, depending on the orientations of the temperature gradient, magnetic field, and voltage. When the magnetic field is applied perpendicularly to the temperature gradient (along the *x*-axis), a voltage drop can be generated along the *y*-axis, known as the transverse-MTE or the Nernst effect. The hallmark of the Nernst effect is the involvement of both electrons and holes within a single material, making it feasible to manufacture a transverse-thermoelectric device using only one type of material.[14]

Previous studies on the Nernst effect have mainly focused on single-crystal materials, such as Cd_3As_2, $PtSn_4$, and Mg_2Pb,[14–16] due to their susceptibility to defects. However, compared to single-crystal materials, polycrystalline materials are easier to fabricate and more promising for practical applications. Consequently, studies on MTE effects in polycrystalline materials have attracted significant attention in recent years. For instance, Feng *et al.* reported that polycrystalline $Mg_{3+\delta}Bi_2$:Mn_x exhibits a significant transverse thermopower of 617 μV K^{-1} and a power factor of 20 393 μW m^{-1} K^{-2} under a 14 T magnetic field at 14 K.[17] This remarkable performance is attributed to the modulation of chemical pressure through Mn doping, resulting in the transition from a topological insulator to a Dirac semimetal. Li *et al.* revealed that, due to the electron–hole compensation and phonon-drag effect, polycrystalline $NbSb_2$ achieves a high transverse thermopower of 396 μV K^{-1} under a 9 T magnetic field at 21 K.[18]

These results indicate that MTE materials are predominantly topological semimetals, characterized by linearly dispersed low-energy excitations and unique topological surface states. The presence of massless Weyl and Dirac quasiparticles typically results in ultra-high carrier mobility, which is beneficial for MTE properties. Furthermore, there are also some narrow-band-gap semiconductors exhibiting high transverse thermoelectric performance, such as $Bi_{77}Sb_{23}$ (E_g = 4.4 meV)[19] and Re_4Si_7 (E_g = 120 meV).[20] The change of Hall mobility induced by Te-doping in $Bi_{77}Sb_{23}$ and the coexistence of electrons and holes in different bands, which is called the multi-carrier mechanism, in the near-intrinsic semiconductor Re_4Si_7 result in the enhanced transverse thermoelectric performance. For the narrow-band-gap semiconductor $Ag_{2-\delta}Te$, on one hand, according to Abrikosov's theory, it exhibits a crossed linear band when doped near 100 K.[21] On the other hand, $Ag_{2-\delta}Te$ (E_g = 50 meV) exhibits an electronic mobility of approximately 8000

[a]*State Key Laboratory of Catalysis, CAS Center for Excellence in Nanoscience, Dalian Institute of Chemical Physics, Chinese Academy of Sciences, Dalian 116023, Liaoning, China. E-mail: pengjiang@dicp.ac.cn; xhbao@dicp.ac.cn*

[b]*University of Chinese Academy of Sciences, Beijing 100049, China*

[c]*Department of Materials Science and Engineering, Southern University of Science and Technology, Shenzhen 518055, Guangdong, China*

[d]*Dalian National Laboratory for Clean Energy, Dalian Institute of Chemical Physics, Chinese Academy of Sciences, Dalian 116023, Liaoning, China*

† Electronic supplementary information (ESI) available. See DOI: https://doi.org/10.1039/d3ta07394g

‡ These authors contributed equally to the work.

$cm^2\ V^{-1}\ s^{-1}$ at 300 K,[22] which is related to the narrow-band-gap electronic structure near room temperature. In general, the Nernst effect is influenced by the carrier mobility and the band structure.[23] On one hand, the magnetic effect, including the Nernst effect, is influenced by the parameter $eB\tau/m^*$ which can be enhanced by the high magnetic field B and high carrier mobility $\mu = e\tau/m^*$ simultaneously, where e is the electronic charge, τ is the relaxation time and m^* is the effective mass, respectively.[24] On the other hand, in non-magnetic semimetal materials, electron–hole compensation, small Fermi surfaces, and high carrier mobility arising from the crossed linear band will be beneficial for enhancing the Nernst effect.[25,26] Consequently, the narrow-band-gap semiconductor $Ag_{2-\delta}Te$ might exhibit promising MTE properties.

Herein, we observe that polycrystalline $Ag_{2-\delta}Te$ exhibits a peak transverse-MTE value of 625 $\mu V\ K^{-1}$ at 75 K, along with a peak transverse power factor of 532 $\mu W\ m^{-1}\ K^{-2}$ at 300 K. Consequently, $Ag_{2-\delta}Te$ exhibits an average Z_N value of $2.9 \times 10^{-4}\ K^{-1}$ over a wide temperature range of 80–300 K. These results highlight the promising potential of Ag_2Te-based materials for thermoelectric conversion applications utilizing the Nernst effect. These findings also provide a new pathway for discovering novel MTE polycrystalline materials.

Experimental section

Material synthesis

Polycrystalline $Ag_{2-\delta}Te$ samples were prepared by melting high purity Ag shots (99.99 wt%, Beijing ZhongNuo Advanced Materials) and Te lumps (99.999 wt%, Beijing ZhongNuo Advanced Materials) together in vacuum-sealed quartz ampoules at a temperature of 1273 K for a duration of 10 hours. Stoichiometric amounts of Ag and Te were weighed according to the nominal compositions of $Ag_{2-\delta}Te$ ($\delta = 0$, 0.005, 0.01, 0.02). The as-cast ingots were subjected to a quenching process in cold water, followed by annealing at a temperature of 700 K for 3 days. The annealed ingots were then ground into fine powders using an agate mortar. Spark plasma sintering (SPS) was employed to consolidate the powders at 700 K under 50 MPa for 10 minutes. The resulting SPS bulks had a diameter of 10 mm and a thickness of 4 mm. To facilitate subsequent characterization, the sintered compacts were cut into various geometries using a diamond wire cutting machine. The relative densities of the sintered samples exceeded 97%.

Material characterization

The phase structure was determined using X-ray diffraction (XRD) with Cu Kα radiation ($\lambda = 1.5406$ Å) at room temperature. XRD measurements were performed on a SmartLab instrument. The temperature-dependent thermal conductivity was measured using the thermal transport option (TTO) on a Quantum Design Physical Property Measurement System (PPMS 14 T). The measurement configuration involved a one-heater and two-thermometer setup. Simultaneous measurements of the transverse and longitudinal thermopower were carried out using a custom sample geometry on the same PPMS system. The heat flow occurred between the hot and cold thermometers which were attached to the lower side of the sample. The transverse voltage leads were deliberately offset to allow for the measurement of both the longitudinal (Seebeck) and transverse (Nernst) voltages. It should be emphasized that, considering the inhomogeneous distribution of the sample temperature due to the voltage offset and the thermal hall effect, the inaccuracies of Seebeck and Nernst coefficients are about 20% and 10%, respectively. The longitudinal and Hall resistivities were determined using the four-probe alternating current transport option (ACT) on the PPMS system.

Results and discussion

Ag_2Te has a monoclinic crystal structure and belongs to the space group $P2_1/c$.[27] $Ag_{2-\delta}Te$, with a slightly excessive Te content, has the same lattice structure as the stoichiometric Ag_2Te and exhibits significant magnetoresistance ($MR = [\rho_{xx}(B) - \rho_{xx}(0\ T)]/\rho_{xx}(0\ T)$) effect.[28] Since a positive correlation exists between MR and MTE effects,[17] a series of $Ag_{2-\delta}Te$ samples with nominal compositions of $Ag_{2-\delta}Te$ ($\delta = 0$, 0.005, 0.01, and 0.02) were synthesized to optimize the MR effect. Since the maximum MR value of $Ag_{2-\delta}Te$ occurs around 100 K,[29] Fig. 1a compares the maximum MR of polycrystalline $Ag_{2-\delta}Te$ samples with different nominal compositions ($\delta = 0$, 0.005, 0.01, and 0.02) around 100 K under a magnetic field of 9 T. Through the defect engineering strategy proposed by Feng *et al.*,[30] the MR of $Ag_{2-\delta}Te$ at 100 K under 9 T increases from 317% to 741%, 822%, and 733% as the nominal Ag-deficient content δ increases from 0 to 0.005, 0.01, and 0.02, respectively. Moreover, as shown in Fig. 1b, the XRD patterns at room temperature confirm that the samples belong to the monoclinic phase and space group $P2_1/c$. However, with δ increasing to 0.02, the excessive Te in sample #4 results in the appearance of Ag_5Te_3 impurities. Therefore, the pure phase sample #3, with a nominal composition of $Ag_{1.99}Te$, exhibiting a maximum MR value of 822% at around 100 K under 9 T, is selected for the subsequent studies.

Fig. 2a displays the temperature-dependent transverse-MTE properties of polycrystalline $Ag_{2-\delta}Te$ (sample #3) with a nominal composition of $Ag_{1.99}Te$. The transverse thermopower was measured with the temperature gradient (dT/dx) along the x-axis, voltage (V) along the y-axis, and magnetic field (B) along the z-axis as illustrated in Fig. 2a. As shown in Fig. 2a, the transverse thermopower (S_{xy}) increases with the increase of the magnetic field and reaches a peak value of 625 $\mu V\ K^{-1}$ under 14 T at 75 K. This value is much higher compared to previously reported values for another silver chalcogenide, Ag_2Se, and is comparable to the S_{xy} values of other outstanding transverse thermoelectric materials,[14–19,30–34] such as polycrystalline $Mg_{3+\delta}Bi_2$:Mn_x (617 $\mu V\ K^{-1}$ under 14 T at 14 K) and single-crystal $NbSb_2$ (616 $\mu V\ K^{-1}$ under 9 T at 25 K) (Fig. 2b).

In order to understand the mechanism of magnetic-field enhanced S_{xy} in polycrystalline $Ag_{2-\delta}Te$, Hall resistivities and Seebeck coefficients were measured. The temperature-dependent Hall resistivity (ρ_{xy}) (Fig. S1a†) and Seebeck coefficient (S_{xx}) (Fig. S1b†) approach zero near 75 K, where the N–P transition occurs,[35] indicating nearly symmetrical electron and

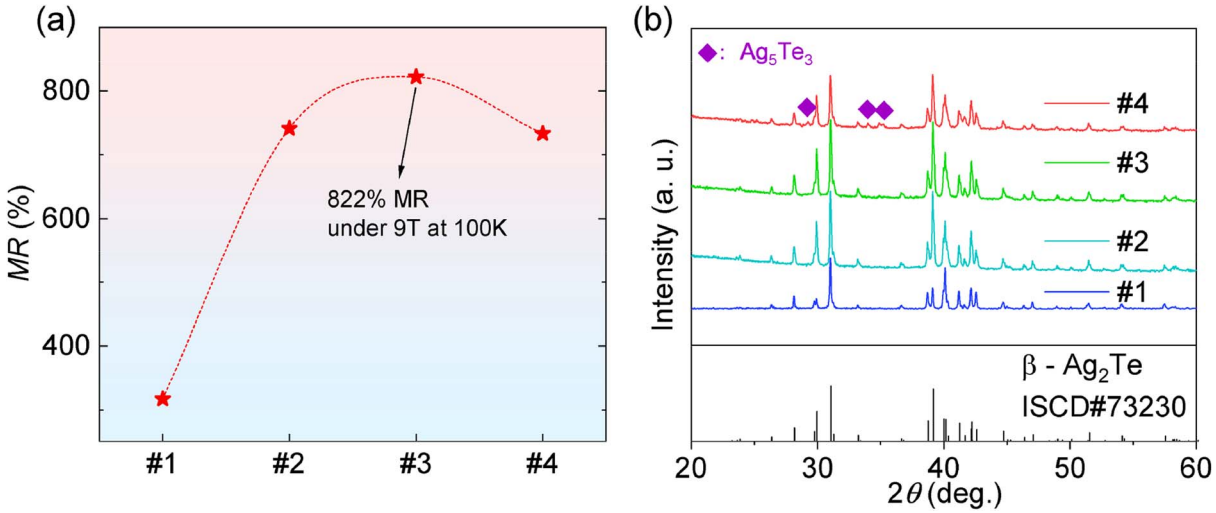

Fig. 1 (a) The MR measured under 9 T at 100 K, and (b) XRD patterns (at 300 K) of $Ag_{2-\delta}Te$ samples [sample #1 ($\delta = 0$), #2 ($\delta = 0.005$), #3 ($\delta = 0.01$), and #4 ($\delta = 0.02$)].

hole transport. Furthermore, as a narrow-gap semiconductor (~50 meV, about $2k_BT$ at 300 K),[36] the bipolar effect is inherent in $Ag_{2-\delta}Te$.[16] In the longitudinal mode, the bipolar effect induces the decrease of the Seebeck coefficient. However, in the transverse mode, the electrons and holes are driven towards opposite directions under the magnetic field, which can enhance the Nernst effect. According to the simplified bipolar transport model with a single conduction band and a single valence band,[16] the transverse thermopower S_{xy} increases with increasing the magnetic field. Additionally, at a specific magnetic field, when the conductivities of electrons and holes are equal, the value of S_{xy} is maximized.[16] As a result, S_{xy} reaches its peak value near the N–P transition temperature (~75 K) (Fig. 2a), which is attributed to the nearly symmetric transport of electrons and holes. The peak position of S_{xy} shifts towards higher temperature with increasing the magnetic field, which is consistent with the behavior of the N–P transition, as shown in Fig. S1a and b.† As temperature increases, $Ag_{2-\delta}Te$ changes to an N-type semiconductor (Fig. S1a†) with electrons as the majority carrier. In the range of 75–200 K, the resistivity decreases with temperature (Fig. 3a), which is a general behavior of a narrow-gap semiconductor. Due to the increased electron concentration from thermal excitation, the contribution of electrons to the conductivity gradually exceeds that of holes. The partial conductivity ratio (σ_e/σ_h) gradually departs from 1 as temperature increases. As a result, the enhancement of the Nernst effect *via* the bipolar effect gradually disappears in the range from 75 to 200 K (Fig. 2a). When the temperature

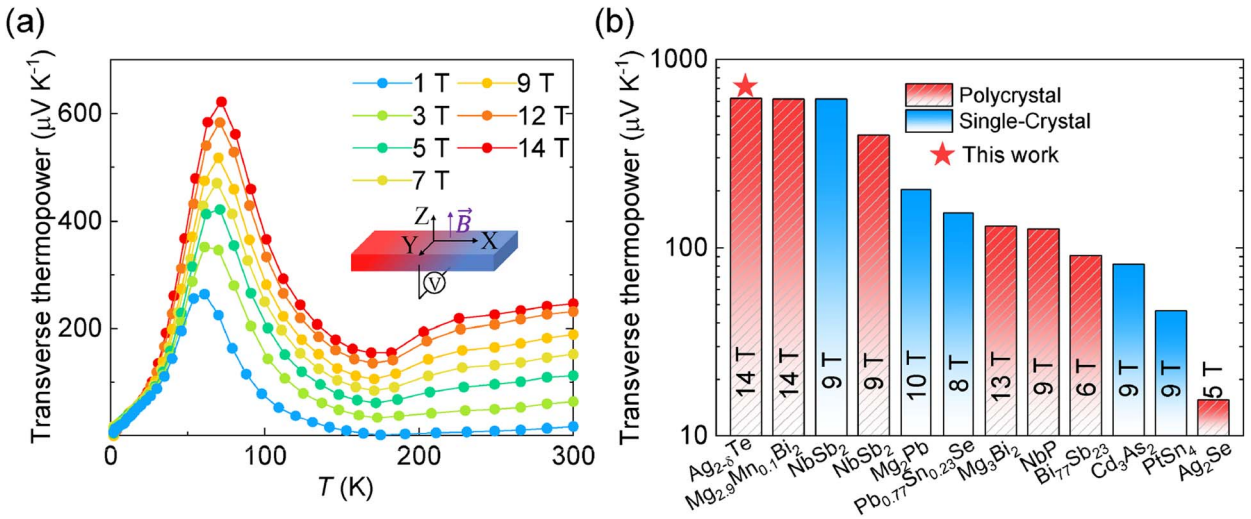

Fig. 2 Transverse thermopower properties of $Ag_{2-\delta}Te$. (a) Temperature dependent transverse thermopower under a magnetic field from 1 T to 14 T. (b) The comparation of the optimal transverse thermopower between our work ($Ag_{2-\delta}Te$) and other materials. Including some single-crystal materials ($PtSn_4$,[15] Cd_3As_2,[14] $Pb_{0.77}Sn_{0.23}Se$,[32] Mg_2Pb,[16] and $NbSb_2$ (ref. 31)) and some polycrystal materials (Ag_2Se,[33] $Bi_{77}Sb_{23}$,[19] NbP,[34] Mg_3Bi_2,[30] $NbSb_2$,[18] and $Mg_{3+\delta}Bi_2$:$Mn_{0.1}$ (ref. 17)).

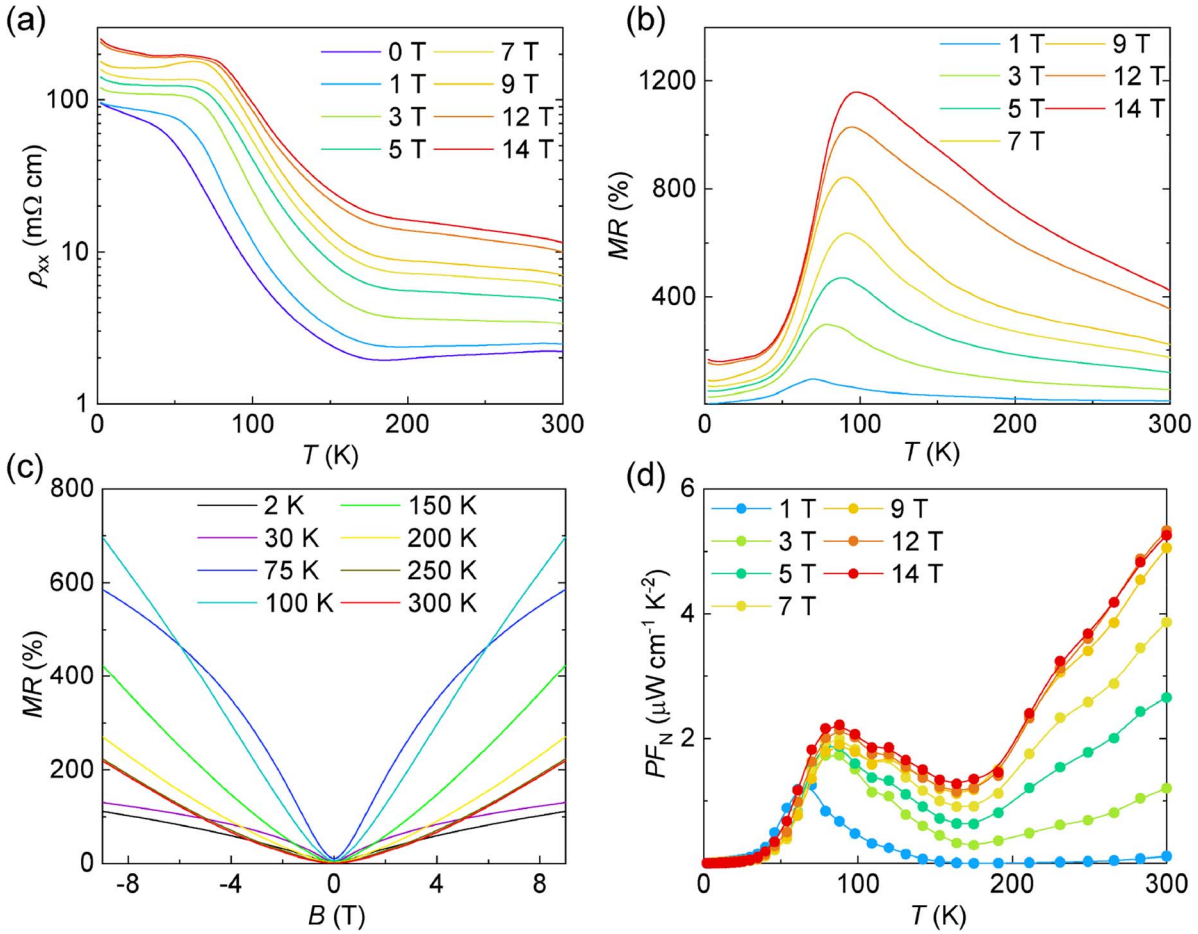

Fig. 3 The electrical properties and the corresponding transverse power factors of $Ag_{2-\delta}Te$. The temperature dependence of (a) the resistivity ρ_{xx}, (b) the MR and (d) the transverse power factor PF_N under various magnetic fields. (c) The magnetic field dependence of the MR at 2–300 K.

reaches 200 K, due to the narrow bandgap (~50 meV) of $Ag_{2-\delta}Te$, the holes as minority carriers can be excited,[24] leading to a turning point in the temperature-dependent resistivity (Fig. 3a). At the same time, the transverse thermopower also shows a turning point near 200 K, followed by a slow increase in the range of 200 to 300 K as the temperature increases (Fig. 2a). This may be attributed to the change of mobility and the thermally excited hole carriers. The simplified bipolar transport model can explain the change of S_{xy} above 200 K.[16] In the high-field limit ($\mu B > 1$), assuming an ideal intrinsic semiconductor model where the concentrations and conductivities of electrons and holes are equal, the S_{xy} can be expressed as:[16]

$$S_{xy} = \frac{S_{e,xy}}{2} + \frac{S_{h,xy}}{2} + \frac{\mu B(S_{h,xx} - S_{e,xx})}{2} \quad (1)$$

where $S_{e,xy}$ and $S_{h,xy}$ are the transverse thermopower of electrons and holes, and $S_{e,xx}$ and $S_{h,xx}$ are the longitudinal thermopower of electrons and holes, respectively. The transverse thermopower under a magnetic field is primarily influenced by the last term, which increases in proportion in the total transverse thermopower as the magnetic field increases. According to the Boltzmann transport model, $S_{h,xx}$ increases with the temperature.[37] Due to the opposite signs of $S_{h,xx}$ and $S_{e,xx}$, the value of $(S_{h,xx}-S_{e,xx})$ gradually increases with temperature. Additionally, when the temperature is above 200 K, though the minority holes can be excited, the magnetic-field-dependent Hall resistivity shows a nearly linear behavior (Fig. S2a†), suggesting a predominantly single-carrier behavior. Hence, the Hall carrier concentration and Hall mobility can be derived using the following formulae.

$$R_H = \frac{\rho_{xy}}{B} \quad (2)$$

$$n_H = \frac{1}{R_H \cdot e} \quad (3)$$

$$\mu_H = \frac{R_H}{\rho_{xx}} \quad (4)$$

R_H, n_H, μ_H, e and ρ_{xx} represent the Hall coefficient, Hall carrier concentration, Hall mobility, elementary charge, and resistivity along the temperature gradient direction, respectively. The results are shown in Fig. S2b.† The Hall carrier mobility decreases from 6944 cm^2 V^{-1} s^{-1} at 200 K to 3932 cm^2 V^{-1} s^{-1} at 300 K. Finally, along with the gradual increase of the value of $(S_{h,xx}-S_{e,xx})$ with temperature as mentioned before, the

transverse thermopower shows a slow increase in the range of 200 to 300 K as the temperature increases.

Additionally, based on the magnetic-field-dependent transverse thermopower values shown in Fig. S3a,† the magnetic-field-dependent Nernst coefficients are displayed in Fig. S3b† by utilizing the relationship $N_{xy} = S_{xy}/\mu_0 H$.[38] The Nernst coefficient (N_{xy}) decreases gradually as the magnetic field increases below 100 K. This behavior is also observed in other transverse-MTE materials.[30] However, when the temperature is above 100 K, the N_{xy} initially increases and then gradually decreases with increasing the magnetic field (Fig. S3b†). There are two possible reasons for such behavior of N_{xy}. On one hand, $Ag_{2-\delta}Te$ exhibits electron-dominated extrinsic semiconductor properties within this temperature range (Fig. S2a†), which allows the N_{xy} to reach the maximum value when $\mu B = 1$.[39] On the other hand, $Ag_{2-\delta}Te$ also has semi-metallic characteristics, such as a narrow bandgap (tens of meV) and relatively large carrier mobility (thousands of $cm^2\ V^{-1}\ S^{-1}$, as shown in Fig. S2b†), which lead to a constant value of N_{xy} when $\mu B > 1$.[39]

Fig. 3a shows the electrical transport properties of $Ag_{2-\delta}Te$ in the temperature range from 2 to 300 K. Notably, a nearly flat resistivity plateau is observed at temperatures below 50 K in Fig. 3a, and the Hall resistivity (ρ_{xy}) follows a similar trend to the resistivity (Fig. S1a†). Such behavior can be attributed to the presence of a degenerate low-temperature hole gas.[35] Furthermore, in the N–P transition region (50–100 K), the inflection points of these resistivity curves that reflect the N–P transition shift to higher temperatures with increasing magnetic fields. The electron to hole mobility ratio, which varies with the magnetic field, can account for the shift in inflection points.[29] Subsequently, in the temperature range of 100 to 200 K, a general semiconductor behavior appears due to carrier activation, resulting in a decreasing trend in resistivity. Furthermore, once the temperature surpasses 200 K, the resistivity at zero-field reaches a plateau again, due to the degeneracy of the electron gas.[35]

We further investigate the dependence of MR on temperature and the magnetic field. As shown in Fig. 3b, the positive MR is observed across the entire temperature range, and the MR increases with the applied magnetic field. Such behavior is consistent with the previous report for polycrystalline $Ag_{2-\delta}Te$.[29] In addition, the peak MR is observed near the N–P transition temperature at various magnetic fields. Similarly, the temperature of the peak MR shifts to higher temperature with increasing the magnetic field. The maximum MR reaches 1162% at 97 K under 14 T. As shown in Fig. 3c, the field-dependent MR exhibits three distinct types of curves. At low temperatures (2, 30, and 75 K), it exhibits a sublinear field-dependent behavior. At 100 K, a nearly linear field dependence is observed, with the maximum MR occurring at this temperature (Fig. 3b). Then, at high temperatures (150, 200, 250, and 300 K), a superlinear field dependence is observed. Such field-dependent behavior is consistent with the previous report.[40] The chemical potential (φ) influenced by both the magnetic field and temperature may explain the different MR behaviors near the N–P transition temperature.[40] Based on Abrikosov's theories,[21] the φ may lie at the crossing point of the crossed linear bands at 100 K, with the electron–hole symmetry occurring. As a result, the MR-B curve exhibits almost linear behavior in Fig. 3c. Both increasing magnetic field or decreasing temperature would lower the chemical potential, and *vice versa*. At temperatures below 100 K, the chemical potential shifts towards the hole-doped region.[40] When applying a magnetic field, as a P-type semiconductor, the further reduction of chemical potential leads to an increase in hole concentration. Compared to the linear MR, the additional increase in the carrier concentration leads to an extra reduction in resistance, resulting in the sublinear behavior. In contrast, when the temperature exceeds 100 K, as an N-type semiconductor, the lower chemical potential in the electron-doped region caused by the magnetic field would decrease the electron concentration, leading to an extra increase in resistance and a superlinear MR behavior.

Combining the transverse thermopower and resistivity, the transverse power factor (PF_N) can be calculated using the equation[41]

$$PF_N = S_{xy}^2/\rho_{yy} \quad (5)$$

The transverse thermopower, which is perpendicular to the temperature gradient, and the electrical resistivity along the *y*-axis, which is also perpendicular to the temperature gradient, are denoted by S_{xy} and ρ_{yy}, respectively. Considering the isotropic electrical resistivity of polycrystalline $Ag_{2-\delta}Te$, ρ_{yy} is expected to be equal to ρ_{xx}. The calculated PF_N values under various magnetic fields are presented in Fig. 3d. When the temperature is between 75 K and 200 K, the transverse power factors of $Ag_{2-\delta}Te$ increase with increasing magnetic fields. When the temperature is above 200 K, they gradually saturate with the magnetic field. The highest PF_N of 532 $\mu W\ m^{-1}\ K^{-2}$ at 300 K under 12 T and a peak PF_N of 222 $\mu W\ m^{-1}\ K^{-2}$ at 85 K under 14 T are attributed to relatively low resistivity and high transverse thermopower, respectively. As shown in Fig. S4,† PF_N almost saturates at 3 T below 100 K, and the saturation magnetic field can reach 9 T above 150 K. Hence, the polycrystalline $Ag_{2-\delta}Te$ can achieve a saturated PF_N under relatively low magnetic fields at low temperatures, and it can also attain higher PF_N under relatively high magnetic fields at high temperatures.

Fig. 4a illustrates the temperature-dependent thermal conductivity (κ_{xx}) of polycrystalline $Ag_{2-\delta}Te$. These measurements were carried out by employing the four-probe method. It is worth noting that the κ_{xx} exhibits similar behavior under different magnetic fields. Specifically, κ_{xx} increases first with the temperature, reaching a maximum value of approximately 10 $W\ m^{-1}\ K^{-1}$ at 10 K. Subsequently, it declines as the temperature increases to about 150 K. Finally, a gradual upward trend is observed until the temperature reaches 300 K. As shown in Fig. 4a, when the temperature is below 50 K, the κ_{xx} remains almost constant with varying magnetic fields, indicating that the thermal conductivity is primarily governed by the lattice thermal conductivity (κ_l) in this temperature range. The κ_l is mainly influenced by the heat capacity, which follows a T^3 dependence according to the Einstein model. As the temperature increases, the κ_l exhibits a T^{-1} dependence due to the enhanced phonon–phonon scattering. Consequently, the thermal conductivities change from a κ_l–T^3 dependence at low

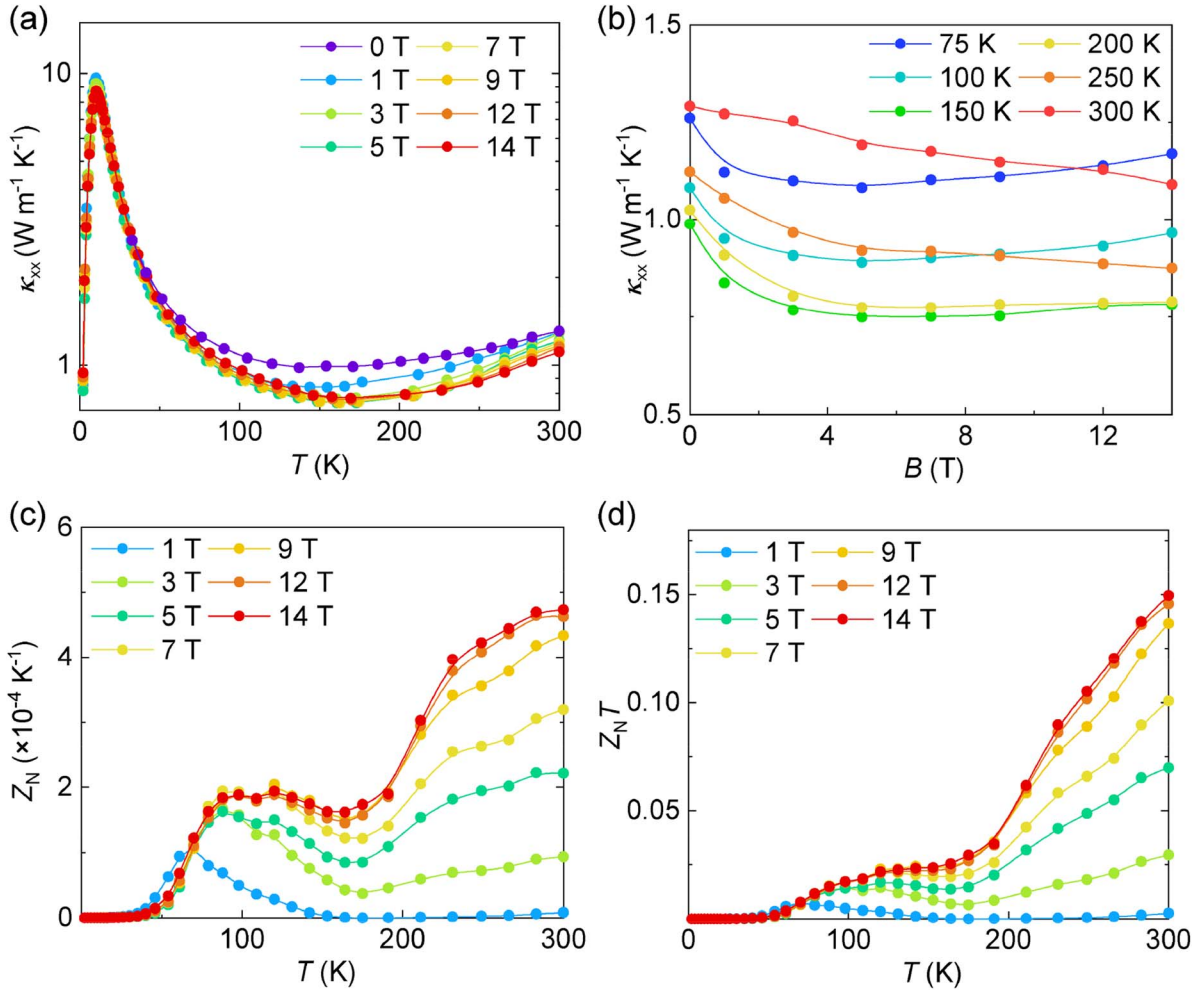

Fig. 4 The thermal conductivity κ_{xx} (a), the transverse thermoelectric figure of merit Z_N (c) and $Z_N T$ (d) under various magnetic fields over the investigate temperature range. The magnetic-field-dependent thermal conductivity (b) at different temperatures.

temperatures to a κ_l–T^{-1} dependence at high temperatures.[31] At 300 K, the κ_{xx} is approximately 1.3 W m^{-1} K^{-1}, which is comparable with the thermal conductivity of conventional thermoelectric materials like Bi_2Te_3 (1.1 W m^{-1} K^{-1})[42] and Cu_2Se (1.0 W m^{-1} K^{-1}).[43] Furthermore, the κ_{xx} remains at around 1 W m^{-1} K^{-1} within the range of 75–300 K. Such relatively low thermal conductivity of polycrystalline $Ag_{2-\delta}Te$ benefits the value of Z_N. When a magnetic field is applied, the κ_{xx} of polycrystalline $Ag_{2-\delta}Te$ above 150 K decreases. As shown in Fig. 4b, the κ_{xx} at 150 K decreases from 0.99 W m^{-1} K^{-1} to 0.75 W m^{-1} K^{-1} with the magnetic field increasing up to 5 T. Then it saturates under higher magnetic fields. When a magnetic field is applied, it can affect the motion and scattering of charge carriers, resulting in a decrease of the thermal conductivity.[31] However, when the temperature is lower than 150 K, the higher field over 5 T enhances the κ_{xx} again (Fig. 4b). The thermal conductivity of polycrystalline $Ag_{2-\delta}Te$ predominantly consists of two components: the lattice part (κ_l) and the electronic part (κ_e).[44] The magnetic field has a minor influence on the lattice part (κ_l). Therefore, the variations in the thermal conductivity under the magnetic field are solely attributed to the change of the electronic part (κ_e). As previously mentioned, in the crossed linear bands of doped Ag_2Te, the chemical potential (φ) is influenced by both the magnetic field and temperature. Both decreasing the temperature and enhancing the magnetic field would lower the φ and *vice versa*. When the temperature is around 100 K, increasing the magnetic field significantly suppresses the contribution of charge carriers at a low magnetic field. As the magnetic field continues to increase, this effect saturates, as is observed at high temperatures. In addition, the further reduced chemical potential due to the increasing magnetic field shifts towards the hole-doped region, increasing the concentration of carriers involved in the thermal conductivity. As a result, the thermal conductivity exhibits a slight increase at high magnetic fields below 150 K.

The Nernst figure-of-merit (Z_N) can be expressed by $Z_N = S_{xy}^2/(\rho_{yy} \cdot \kappa_{xx})$. The Z_N and corresponding $Z_N T$ of polycrystalline $Ag_{2-\delta}Te$ under different magnetic fields are shown in Fig. 4c and d, respectively. Below 150 K, a peak value of Z_N is observed around 100 K, followed by an increase in Z_N with the further increasing temperature, which is consistent with the transverse power factor behavior (Fig. 3d). After introducing the temperature parameter,

Z_NT increases with temperature up to 300 K. Due to the increased transverse power factor and decreased thermal conductivity in polycrystalline $Ag_{2-\delta}Te$, the Z_N shows a remarkable increase when a magnetic field is applied. Specifically, at temperatures below 150 K, a peak Z_N value of 2×10^{-4} K^{-1} is achieved under 7 T at 100 K. Moreover, at 300 K, the maximum Z_N value reaches 4.7×10^{-4} K^{-1} under 14 T, corresponding to a peak Z_NT of 0.15. The saturated magnetic field for Z_N and Z_NT exhibits similar behavior, increasing from 3 T at 75 K to 14 T at 300 K (Fig. S5a and b†). Such behaviors can be attributed to the variation in the saturated magnetic field of PF_N and κ_{xx} with temperature observed before (Fig. 3d and 4a). The Z_NT near room temperature of narrow-band-gap semiconductors, Re_4Si_7 (ref. 20) and $Bi_{77}Sb_{23}$,[19] is 0.1 at 400 K and 0.06 at 300 K, respectively. The Z_NT value 0.15 of $Ag_{2-\delta}Te$ in this work is comparable with those of state-of-the-art transverse thermoelectric materials, indicating that $Ag_{2-\delta}Te$ is a promising material for MTE applications.

For practical applications of transverse thermoelectric materials, besides the maximum peak Z_N, a high average Z_N over a wide temperature range is even more meaningful. Table S1† presents the average Z_N values reported in previous literature, obtained by integrating the temperature-dependent Z_N values over the measured temperature range and dividing by the temperature difference (ΔT). The average Z_N values of single crystals are relatively large. However, the optimal performance temperature range is usually very narrow. For instance, the average Z_N values of WTe_2 and $NbSb_2$ are 193×10^{-4} K^{-1} at 7–16 K and 26.6×10^{-4} K^{-1} at 5–70 K, respectively. Furthermore, the large-scale synthesis of high-quality single-crystal materials remains challenging. In contrast, polycrystalline samples have a relatively wide applicable temperature range. For example, the average Z_N values of Ag_2Se,[33] $Bi_{77}Sb_{23}$ (ref. 19) and $NbSb_2$ (ref. 18) are 0.23×10^{-4} K^{-1} at 80–300 K, 2.15×10^{-4} K^{-1} at 50–300 K and 9.75×10^{-4} K^{-1} at 5–100 K, respectively. From liquid nitrogen temperature to room temperature, $Ag_{2-\delta}Te$ is comparable with the state-of-the-art transverse thermoelectric material $Bi_{77}Sb_{23}$ and shows a 12-fold improvement compared to Ag_2Se, which is also a polycrystalline silver chalcogenide material.

Conclusions

In this work, we investigate the transverse magneto-thermoelectric properties of polycrystalline $Ag_{2-\delta}Te$. We observe a significant peak value of transverse thermopower of 625 μV K^{-1} at 75 K under a magnetic field of 14 T, which can be attributed to the enhanced bipolar effect near the N–P transition temperature. An average Z_N value of 2.9×10^{-4} K^{-1} over a wide temperature range of 80–300 K under a magnetic field of 14 T is achieved. These results suggest that polycrystalline $Ag_{2-\delta}Te$ holds great promise for transverse energy conversion applications due to its relatively high transverse thermoelectric performances.

Author contributions

Mingyu Chen: material synthesis, sample testing, data analysis, and writing & editing, Tao Feng: PPMS measurement and review, Nan Yin: support for PPMS measurement, Quan Shi: support for PPMS measurement, Peng Jiang: conceptualization, supervision, writing, and review & editing, and Xinhe Bao: review & editing.

Conflicts of interest

The authors declare that they have no known competing financial interests or personal relationships that could have appeared to influence the work reported in this paper.

Acknowledgements

This work was supported by the National Key R&D Program of China (2022YFA1203600), CAS Interdisciplinary Innovation Team (JCTD-2019-08), and DNL Cooperation Fund (DNL202018). We thank Wenqing Zhang from the Southern University of Science and Technology for helpful discussions.

References

1 Q. Y. Yan and M. G. Kanatzidis, *Nat. Mater.*, 2022, **21**, 503–513.
2 J. Mao, G. Chen and Z. F. Ren, *Nat. Mater.*, 2021, **20**, 454–461.
3 W. N. Zhou, K. Yamamoto, A. Miura, R. Iguchi, Y. Miura, K. Uchida and Y. Sakuraba, *Nat. Mater.*, 2021, **20**, 463–467.
4 Y. Z. Pei, A. D. LaLonde, N. A. Heinz, X. Y. Shi, S. Iwanaga, H. Wang, L. D. Chen and G. J. Snyder, *Adv. Mater.*, 2011, **23**, 5674–5678.
5 W. Liu, X. J. Tan, K. Yin, H. J. Liu, X. F. Tang, J. Shi, Q. J. Zhang and C. Uher, *Phys. Rev. Lett.*, 2012, **108**, 166601.
6 G. J. Tan, F. Y. Shi, S. Q. Hao, H. Chi, T. P. Bailey, L. D. Zhao, C. Uher, C. Wolverton, V. P. Dravid and M. G. Kanatzidis, *J. Am. Chem. Soc.*, 2015, **137**, 11507–11516.
7 Y. Z. Pei, Z. M. Gibbs, A. Gloskovskii, B. Balke, W. G. Zeier and G. J. Snyder, *Adv. Energy Mater.*, 2014, **4**, 1400486.
8 S. Roychowdhury, T. Ghosh, R. Arora, M. Samanta, L. Xie, N. K. Singh, A. Soni, J. Q. He, U. V. Waghmare and K. Biswas, *Science*, 2021, **371**, 722–727.
9 K. Biswas, J. Q. He, Q. C. Zhang, G. Y. Wang, C. Uher, V. P. Dravid and M. G. Kanatzidis, *Nat. Chem.*, 2011, **3**, 160–166.
10 R. G. Deng, X. L. Su, Z. Zheng, W. Liu, Y. G. Yan, Q. J. Zhang, V. P. Dravid, C. Uher, M. G. Kanatzidis and X. F. Tang, *Sci. Adv.*, 2018, **4**, eaar5606.
11 S. I. Kim, K. H. Lee, H. A. Mun, H. S. Kim, S. W. Hwang, J. W. Roh, D. J. Yang, W. H. Shin, X. S. Li, Y. H. Lee, G. J. Snyder and S. W. Kim, *Science*, 2015, **348**, 109–114.
12 J. P. Heremans, C. M. Thrush and D. T. Morelli, *Phys. Rev. B: Condens. Matter Mater. Phys.*, 2004, **70**, 115334.
13 C. C. Zhao and C. Xiao, *Rare Met.*, 2021, **40**, 752–766.
14 J. S. Xiang, S. L. Hu, M. Lyu, W. L. Zhu, C. Y. Ma, Z. Y. Chen, F. Steglich, G. F. Chen and P. J. Sun, *Sci. China: Phys., Mech. Astron.*, 2020, **63**, 237011.
15 C. G. Fu, S. N. Guin, T. Scaffidi, Y. Sun, R. Saha, S. J. Watzman, A. K. Srivastava, G. W. Li, W. Schnelle, S. S. P. Parkin, C. Felser and J. Gooth, *Research*, 2020, **2020**, 4643507.

16 Z. W. Chen, X. Y. Zhang, J. Ren, Z. Z. Zeng, Y. Chen, J. He, L. D. Chen and Y. Z. Pei, *Nat. Commun.*, 2021, **12**, 3837.
17 T. Feng, P. S. Wang, Z. J. Han, L. Zhou, Z. R. Wang, W. Q. Zhang, Q. H. Liu and W. S. Liu, *Energy Environ. Sci.*, 2023, **16**, 1560–1568.
18 P. Li, P. F. Qiu, J. Xiao, T. T. Deng, L. D. Chen and X. Shi, *Energy Environ. Sci.*, 2023, **16**, 3753–3759.
19 M. Murata, K. Nagase, K. Aoyama and A. Yamamoto, *Appl. Phys. Lett.*, 2020, **117**, 103903.
20 M. R. Scudder, B. He, Y. X. Wang, A. Rai, D. G. Cahill, W. Windl, J. P. Heremans and J. E. Goldberger, *Energy Environ. Sci.*, 2021, **14**, 4009–4017.
21 A. A. Abrikosov, *Phys. Rev. B: Condens. Matter Mater. Phys.*, 1998, **58**, 2788–2794.
22 H. S. Schnyders, *Appl. Phys. Lett.*, 2015, **107**, 042103.
23 R. T. Delves, *Rep. Prog. Phys.*, 1965, **28**, 249–289.
24 I. Yoshida, T. Ono, M. Sakurai and S. Tanuma, presented in part at *XVII International Conference on Thermoelectrics*, Nagoya, Japan, May, 1998.
25 C. G. Fu, Y. Sun and C. Felser, *APL Mater.*, 2020, **8**, 040913.
26 B. H. Yan and C. Felser, *Annu. Rev. Condens. Matter Phys.*, 2017, **8**, 337–354.
27 A. Vanderlee and J. L. Deboer, *Acta Crystallogr., Sect. C: Cryst. Struct. Commun.*, 1993, **49**, 1444–1446.
28 R. Xu, A. Husmann, T. F. Rosenbaum, M. L. Saboungi, J. E. Enderby and P. B. Littlewood, *Nature*, 1997, **390**, 57–60.
29 H. S. Schnyders, M. L. Saboungi and T. F. Rosenbaum, *Appl. Phys. Lett.*, 2000, **76**, 1710–1712.
30 T. Feng, P. S. Wang, Z. J. Han, L. Zhou, W. Q. Zhang, Q. H. Liu and W. S. Liu, *Adv. Mater.*, 2022, **34**, 2200931.
31 P. Li, P. F. Qiu, Q. Xu, J. Luo, Y. F. Xiong, J. Xiao, N. Aryal, Q. Li, L. D. Chen and X. Shi, *Nat. Commun.*, 2022, **13**, 7612.
32 T. Liang, Q. Gibson, J. Xiong, M. Hirschberger, S. P. Koduvayur, R. J. Cava and N. P. Ong, *Nat. Commun.*, 2013, **4**, 2696.
33 Y. Z. Lei, W. Liu, X. Y. Zhou, J. F. Luo, C. Zhang, X. L. Su, G. J. Tan, Y. G. Yan and X. F. Tang, *J. Solid State Chem.*, 2020, **288**, 121453.
34 W. Liu, Z. H. Wang, J. H. Wang, H. Bai, Z. Li, J. C. Sun, X. Y. Zhou, J. F. Luo, W. Wang, C. Zhang, J. S. Wu, Y. Sun, Z. W. Zhu, Q. J. Zhang and X. F. Tang, *Adv. Funct. Mater.*, 2022, **32**, 2202143.
35 F. F. Aliev, E. M. Kerimova and S. A. Aliev, *Semiconductors*, 2002, **36**, 869–873.
36 C. Wood, W. M. Kane and V. Harrap, *Phys. Rev.*, 1961, **121**, 978–982.
37 R. T. Delves, *Rep. Prog. Phys.*, 1965, **28**, 249–285.
38 A. Pourret, H. Aubin, J. Lesueur, C. A. Marrache-Kikuchi, L. Berge, L. Dumoulin and K. Behnia, *Phys. Rev. B: Condens. Matter Mater. Phys.*, 2007, **76**, 214504.
39 R. T. Delves, *Br. J. Appl. Phys.*, 1962, **13**, 440–445.
40 Y. Sun, M. B. Salamon, M. Lee and T. F. Rosenbaum, *Appl. Phys. Lett.*, 2003, **82**, 1440–1442.
41 C. G. Fu, S. N. Guin, S. J. Watzman, G. W. Li, E. K. Liu, N. Kumar, V. Suss, W. Schnelle, G. Auffermann, C. Shekhar, Y. Sun, J. Gooth and C. Felser, *Energy Environ. Sci.*, 2018, **11**, 2813–2820.
42 B. Poudel, Q. Hao, Y. Ma, Y. C. Lan, A. Minnich, B. Yu, X. A. Yan, D. Z. Wang, A. Muto, D. Vashaee, X. Y. Chen, J. M. Liu, M. S. Dresselhaus, G. Chen and Z. F. Ren, *Science*, 2008, **320**, 634–638.
43 H. L. Liu, X. Shi, F. F. Xu, L. L. Zhang, W. Q. Zhang, L. D. Chen, Q. Li, C. Uher, T. Day and G. J. Snyder, *Nat. Mater.*, 2012, **11**, 422–425.
44 G. J. Snyder and E. S. Toberer, *Nat. Mater.*, 2008, **7**, 105–114.